Metastable states of dimethyloxonium, $(CH_3)_2OH^\bullet$

František Tureček[*], Philip J. Reid

Department of Chemistry, University of Washington, Bagley Hall, Box 351700, Seattle, WA 98195-1700, USA

Dedicated to Professor Jack E. Beauchamp on the occasion of his 60th birthday.

Abstract

Hypervalent dimethyloxonium radical, $(CH_3)_2O–H^\bullet$ (**1**), is formed by collisional electron transfer to protonated dimethyl ether in the gas phase and dissociates rapidly by cleavage of the O–H and O–C bonds. Ab initio and density functional theory calculations show that these dissociations originate from different electronic states of **1**. The loss of H proceeds from the repulsive ground electronic (X) state of **1** and is $131\,kJ\,mol^{-1}$ exothermic to form vibrationally excited $(CH_3)_2O$. The loss of methyl proceeds from the first excited electronic (A) state of **1** by crossing to the repulsive part of the X state potential energy surface, yielding vibrationally excited methanol. A substantial fraction of deuterated radicals, $(CH_3)_2O–D^\bullet$ (**1**-OD), are metastable on the microsecond time scale. The metastable species result from the population of the B and higher excited states of **1** that are calculated to be bound along both O–H and O–C coordinates. The isotope effects on the metastability of **1** are explained by less efficient vibronic coupling between the bound B and dissociative A states in the deuterated radical. (Int J Mass Spectrom 222 (2003) 49–61)
© 2002 Elsevier Science B.V. All rights reserved.

Keywords: Hypervalent radicals; Neutralization-reionization mass spectrometry; Excited states; Ab initio calculations; Vibronic coupling

1. Introduction

Onium radicals (ammonium, oxonium, phosphonium, sulfonium, etc.) arise by addition of hydrogen atoms or larger radicals to coordinatively saturated heteroatoms (N, O, P, S) in ammonia or amines, water, alcohols or ethers, phosphine or alkylphosphines, and hydrogen sulfide, thiols or sulfides. Since the addition results in the heteroatom having formally nine valence electrons, onium radicals violate the octet rule [1] and are therefore, regarded as hypervalent [2–4]. While the role of hypervalent radicals as intermediates of radical reactions in the condensed phase has been contentious

[5,6], there is a large body of experimental [7–26] and theoretical [27–38] data indicating that some hypervalent radicals do or should exist as metastable species in the gas phase. Starting with Herzberg's study of NH_4 emission bands in discharge in gaseous ammonia [39], simple hypervalent radicals have been considered as intermediates of other high-energy processes, such as dissociative recombination in plasmas [40,41]. Gas-phase hypervalent radicals are formed transiently from stable onium ions by electron capture or collisional electron transfer at kiloelectron volt collision energies. While electron capture results in highly exothermic dissociative recombination [41], collisional electron transfer has shown to yield several remarkably stable species of microsecond lifetimes

---

[*] Corresponding author. E-mail: turecek@chem.washington.edu

[42]. Most of the data on hypervalent radicals has come from neutralization-reionization mass spectrometric (NRMS) studies that have been extensively reviewed [43]. Briefly, a beam of stable onium ions is prepared in a high-pressure ion source and selected by mass. The ions are accelerated to kiloelectron volt kinetic energies (typically 8–10 keV) and allowed to collide with a thermal atomic or molecular gas that serves as an electron donor. Polarizable atoms (Xe, Hg) [43c] or molecules (trimethylamine, dimethyldisulfide) [43f] have been used successfully as electron donors. The remaining cations are removed electrostatically and the radicals are allowed to drift for 100 ns to a few microseconds when dissociation occurs. The mixture of surviving radicals and their neu-

tral dissociation products is ionized without separation to cations by collisions with another gas (typically O_2) and the ions are analyzed by mass spectrometry. The presence of a reionized precursor (survivor ion) is taken as evidence for a metastable hypervalent radical.

The formation, metastability, and dissociations of several hypervalent radicals have been studied previously for a variety of structures and heteroatoms [12–26]. Two unusual phenomena stand out from these studies. First, very large isotope effects have been observed for deuterium substituted hypervalent radicals [15–25]. A striking example is dimethyloxonium, $(CH_3)_2O–H^\bullet$ (**1**) where collisional electron transfer does not result in the formation of a metastable
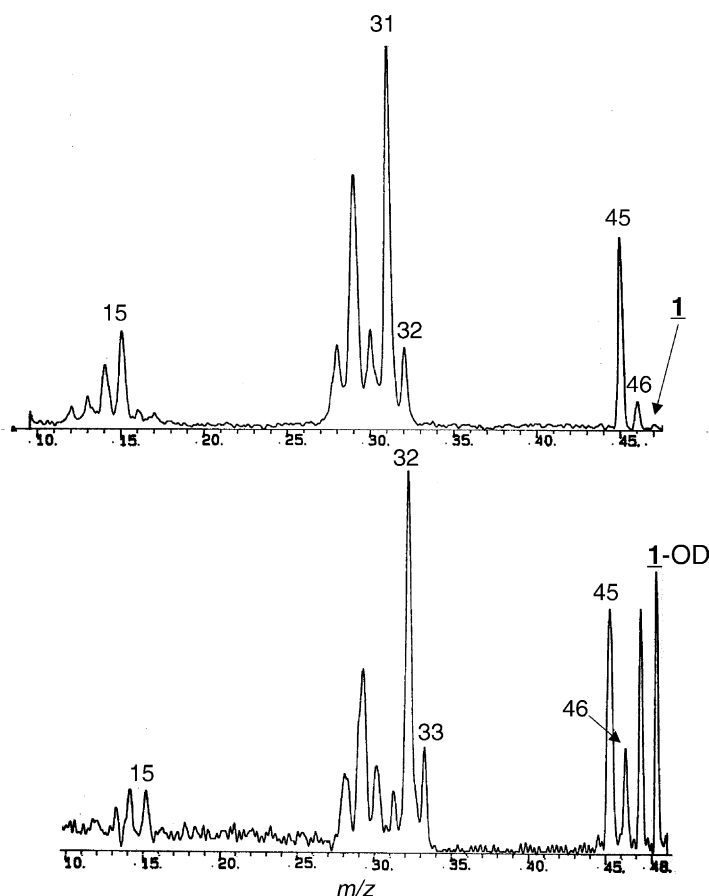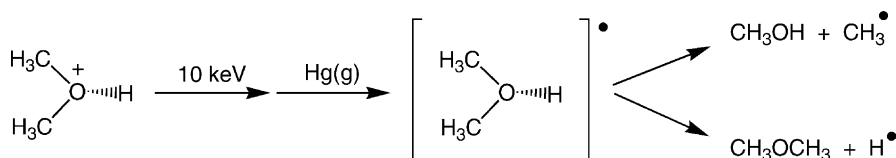

Fig. 1. Hg (70%)/O_2 (70%) neutralization-reionization mass spectra of (top) **1** and (bottom) **1**-OD.

Scheme 1.

radical, such that the survivor ion is missing in the NR mass spectrum [15,19,22]. By contrast, $(CH_3)_2O–D^\bullet$ (**1**-OD) forms a very abundant survivor ion attesting to the metastability of the intermediate hypervalent radical. This large isotope effect was observed for radicals formed by electron transfer from Xe [15,19], *N,N*-dimethylaniline and dimethyl disulfide [22], and Hg, as shown in Fig. 1. Another salient feature of the NR mass spectra is the presence of competing O–(H,D) and O–C bond dissociations. The former results in the formation of dimethyl ether which is detected as the corresponding cation-radical at *m/z* 46 and its dissociation products at *m/z* 45 and 31. Dissociation of the C–O bond forms methanol that is detected at *m/z* 32 and 31, and a methyl radical whose ion signal coincides with those of methanol and dimethyl ether dissociation products (Scheme 1). Preliminary ab initio calculations [22] predicted that radical **1** is unbound along the O–H coordinate, and should dissociate spontaneously and exothermically to dimethyl ether and a hydrogen atom. The observed metastability of **1**-OD and the C–O bond dissociation were therefore incompatible with the calculated energetics.

We have shown previously that dissociations observed in the NR mass spectra of hypervalent radicals can be attributed to the properties of the potential energy surfaces of excited electronic states [18,22,23]. In the present work, we use high-level ab initio calculations to examine the potential energy surfaces of **1**. We show that the dissociations can be readily explained as starting from different electronic states. A more difficult question to address concerns the origin of the deuterium isotope effects on the hypervalent radical's lifetimes.
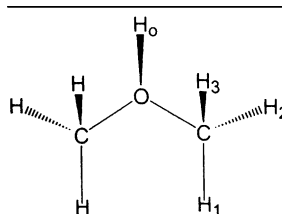
2. Calculations

Standard ab initio calculations were performed using the Gaussian 98 [44] suite of programs. Geometries were optimized with density functional theory calculations using Becke's hybrid functional (B3LYP) [45] and the 6-311+G(2d,p) and 6-311++G(2df,p) basis sets for ions and radicals, respectively. Radical excited state geometries were optimized with configuration interaction singles (CIS) [46] calculations and the 6-31++G(2d,p) basis set. The desired excited electronic state was selected for gradient optimization as the corresponding root of the CI matrix [46]. Spin unrestricted calculations (UCIS) were used for all open-shell systems. Potential energy mapping was performed with UCIS/6-31++G(2d,p) by stepwise calculations in which one internal coordinate was fixed while the others were fully optimized. Stationary points were characterized by harmonic frequency calculations with UCIS/6-31++G(2d,p) as local energy minima (all real frequencies) or first-order saddle points (one imaginary frequency). Improved energies were obtained by single-point calculations using both UCIS and time-dependent density functional theory [47] with the B3LYP functional and the larger 6-311++G(3df,2p) basis set.

3. Results and discussion

3.1. Ground electronic state of **1**

Protonation of dimethyl ether yields a single stable ion (**1**$^+$) of C_s symmetry whose optimized geometry is shown in Table 1. Vertical electron capture in **1**$^+$

Table 1
Optimized geometries

Geometry parameters[a]

	1[+b]	(A) 1[c]	(B) 1[c]	(C) 1[c]	2[d]	3[d]
C–O	1.479 (1.497)[e] (1.497)[d]	1.500	1.482	1.475	1.410	1.832
H_0–O	0.951 (0.975) (0.974)	0.941	0.938	0.938	2.821	0.960
H_1–C	1.077 (1.084) (1.085)	1.076	1.078	1.074	1.099	1.081
H_2–C	1.077 (1.085) (1.086)	1.079	1.075	1.077	1.089	1.083
H_3–C	1.079 (1.086) (1.087)	1.079	1.080	1.077	1.099	1.083
C–O–C	118.2 (115.0) (117.0)	116.5	117.5	120.4	112.9	161.3
H_0–O–C	112.6 (110.3) (111.3)	112.4	112.8	111.2	113.9	99.4
H_1–C–O	105.4 (104.9) (105.2)	104.8	105.4	105.5	111.4	99.3
H_2–C–O	105.8 (105.5) (105.5)	105.9	105.9	104.3	107.4	104.9
H_3–C–O	108.4 (108.7) (108.7)	107.7	108.1	107.5	111.4	104.9
H_0–O–C–C	134.0 (125.6) (129.6)	131.8	134.0	132.7	131.9	180.0
H_1–C–O–C	59.7 (62.7) (61.0)	56.7	65.2	44.6	60.8	0.1
H_2–C–O–C	177.8 (180.5) (178.9)	175.2	183.8	160.9	180.2	119.0
H_3–C–O–C	−61.2 (−58.1) (−59.8)	−63.1	−55.9	−77.0	−60.5	−118.8

[a] Bond lengths in angstroms (Å), bond and dihedral angles in degrees (°).

[b] From HF/6-31++G(2d,p) optimization.

[c] From UCIS/6-31++G(2d,p) optimizations.

[d] From B3LYP/6-311+G(2df,p) optimizations.

[e] From MP2/6-31++G(2d,p) optimization.

forms the various electronic states of radical **1** that were investigated computationally. Attempts to find a local energy minimum for the $^2A'$ ground (X) electronic state of **1** failed. Regardless of the initial geometry estimate for **1**, upon gradient optimization the radical dissociated by cleavage of the O–H bond. A shallow potential energy minimum was found for a loosely bound $(CH_3)_2O \cdots H^\bullet$ van der Waals complex (**2**) that had a long O–H bond (2.82 Å) with a very low stretching frequency, $\nu(OH) = 21\,cm^{-1}$, and was bound against dissociation to $(CH_3)_2O$ and a H atom by $0.2\,kJ\,mol^{-1}$. However, the complex was made unbound upon including zero-point vibrational energy corrections that brought its 0 K energy $0.7\,kJ\,mol^{-1}$ above $(CH_3)_2O + H^\bullet$. In addition to the absence of a potential energy minimum for the $(^2A')$ X state of **1**, the point of vertical landing on the repulsive potential energy surface is ca. $130\,kJ\,mol^{-1}$ above the dissoci-

ation products, $(CH_3)_2O + H^\bullet$, indicating exothermic dissociation within one vibrational period of the O–H bond.

Another stationary point that was located on the $[(CH_3)_2O + H^\bullet]$ radical potential energy surface was a first-order saddle point of C_s symmetry (**3**, Table 1) corresponding to the transition state for the degenerate methyl substitution in methanol (Scheme 2). Transition state **3** was calculated to be $62\,kJ\,mol^{-1}$ above $(CH_3)_2O + H^\bullet$ and $161\,kJ\,mol^{-1}$ above $CH_3OH + CH_3^\bullet$. The calculations, thus, indicate a substantial activation energy for the methyl radical substitution in methanol [5,19].

The present results are consistent with previous calculations that used Moller–Plesset perturbational theory and comparable basis sets to conclude that radical **1** was unbound in its ground electronic state and should dissociate without barrier by cleavage of

Scheme 2.
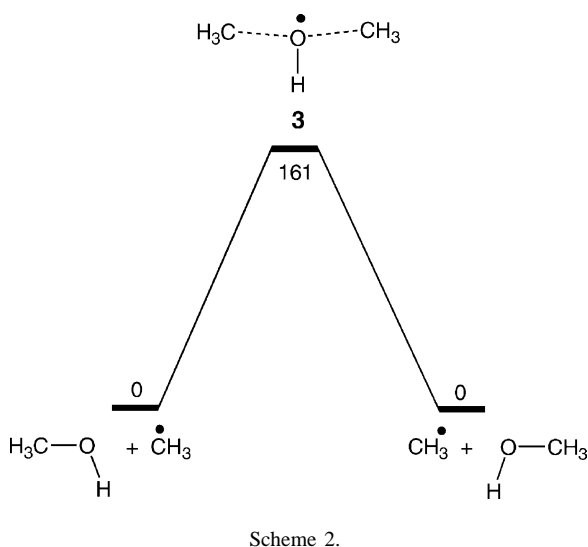
the O–H bond [22]. Interestingly, a shallow potential energy minimum was recently found for $H_3O^\bullet$ which is the lowest homologue of the hypervalent oxonium radical series [38]. This indicates that the methyl groups in **1** destabilize the *X* state of the radical.

The reason for this destabilization can be understood from the radical's electronic structure (Fig. 2). The unpaired electron enters a high-lying orbital (9a′, SOMO, $-\varepsilon = 2.32$ eV) that has a large MO coefficient at the oxonium hydrogen atom and is antibonding along the O–H coordinate. As a result, a substantial electron density is localized on the oxonium hydrogen, as evidenced by its negative atomic charge (-0.53) and high spin density (0.91). The underlying doubly-occupied orbital (8a′, Fig. 2) consist of an antibonding combination of the oxygen p_z atomic orbital with the pseudo-π orbitals of the methyl groups and is similar by energy and nodality to the HOMO in $\mathbf{1^+}$. The properties of the frontier orbitals in **1** are qualitatively similar to those calculated for other hypervalent radicals, namely, dimethylammonium [22], trimethylammonium [18], and alkylmethyloxonium [20].

The potential energy gained by vertical electron transfer forming the repulsive *X* state is estimated from the position of the landing point on the energy scale. The landing point energy is calculated relative to $\mathbf{1^+}$ as $\Delta E = -370$ to -406 kJ mol^{-1} from MP2 and B3LYP
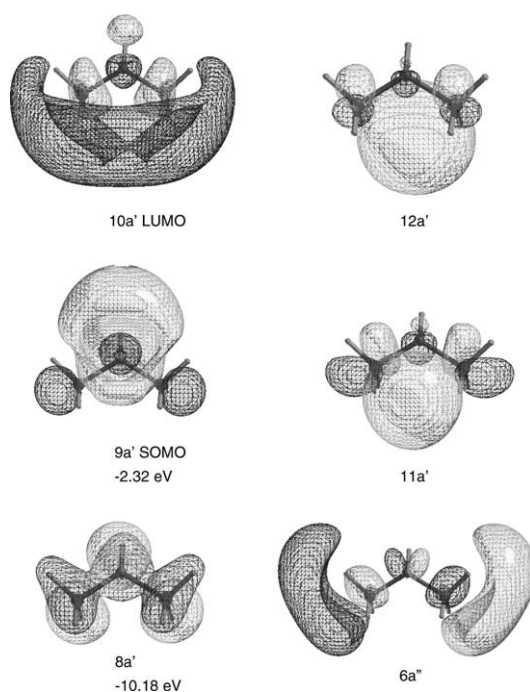

Fig. 2. Frontier molecular orbitals in **1** from B3LYP/6-311+ G(3df,2p) single-point calculation on $\mathbf{1^+}$ optimized geometry. The lowest excited states correspond to electron promotions of 9a′ → 10a′ for the *A* state, 9a′ → 6a″ for the *B* state, 9a′ → 11a′ for the *C* state, and 9a′ → 12a′ for the *D* state of **1**.

calculations, respectively. This gives an average value of 165 kJ mol^{-1} on the $\Delta H_{f,298}$ scale, which according to the product enthalpies of formation [48] places vertically formed **1** at 131 kJ mol^{-1} above $[(CH_3)_2O + H^\bullet]$ and 220 kJ mol^{-1} above $[CH_3OH + CH_3^\bullet]$.

3.2. Excited electronic states of 1

In contrast to the repulsive nature of the *X* state of **1**, there are several bound excited electronic states, as illustrated by the optimized geometries for the $(^2A')A$, $(^2A'')B$, and $(^2A')C$ states (Table 1). The geometries of the excited states are similar to that of ion $\mathbf{1^+}$. For example, the lengths of the O–H and C–O bonds gradually decrease upon electron promotion to higher excited states. According to TD-B3LYP calculations, the excited states arise by promoting the odd electron from the 9a′ orbital to the 10a′ (*A*), 6a″ (*B*), 11a′ (*C*),

Table 2
Calculated excitation energies of **1**

State	Excitation and ionization energy (eV)				
	UCIS/6-31++G(2d,p)	UCIS/6-311++G(3df,2p)	TD-B3LYP/6-311++G(3df,2p)	f[a, b]	τ (μs)[a, c]
Ion geometry					
X	0	0 (3.83)[d]	0 (4.20)[d]	–	–
A	1.21	1.23 (2.60)	1.01 (3.19)	0.0013	17.3
B	1.50	1.51 (2.32)	1.50 (2.71)	0.021	0.49
C	1.79	1.75 (2.08)	1.72 (2.49)	0.11	0.070
D	2.03	2.04 (1.79)	1.84 (2.36)	0.12	0.055
E	2.49	2.49 (1.34)	2.42 (1.79)	0.12	0.033
A-optimized					
X	0	0 (3.69)[e]	0 (4.09)[e]	–	–
A	1.09	1.11 (2.58)	0.94 (3.16)	0.0009	29[f]
B	1.39	1.39 (2.30)	1.43 (2.66)	0.017	–
C	1.65	1.61 (2.08)	1.66 (2.43)	0.11	–
B-optimized					
X	0	0 (3.69)[e]	0 (4.06)[e]	–	–
A	1.14	1.15 (2.54)	0.95 (3.11)	0.0026	–
B	1.39	1.40 (2.29)	1.42 (2.64)	0.03	0.38[f]
C	1.73	1.66 (2.03)	1.65 (2.42)	0.12	–
C-optimized					
X	0	0 (3.64)[e]	0 (4.00)[e]	–	–
A	1.13	1.15 (2.49)	0.97 (3.03)	0.004	–
B	1.43	1.43 (2.20)	1.45 (2.55)	0.032	–
C	1.57	1.54 (2.09)	1.60 (2.40)	0.12	0.072[f]

[a] From TD-UB3LYP/6-311++G(3df,2p) calculations.
[b] Oscillator strengths for transitions to the X state.
[c] Radiative lifetimes for transitions to the X state.
[d] Vertical ionization energies.
[e] Adiabatic ionization energies for the optimized electronic states.
[f] Radiative lifetimes calculated only for the optimized electronic states.

12a′ (D) and 7a″ (E) orbitals. The doubly-occupied 8a′ orbital does not mix with the SOMO and the virtual orbitals in the A–E excited states. This finding justifies the use of CI-singles for the geometry optimizations, because the dominant configurations in the CI matrix involve mainly excitation of the single 9a′ electron.

The excited state energies, as calculated for vertical electron capture in **1$^+$**, and in the optimized geometries of the A–C excited states, are summarized in Table 2. The vertical recombination energy of **1$^+$** to drop to the repulsive X state of **1** is RE_v = 4.2 eV, in good agreement with previous MP2 calculations [22]. The lowest excited states are closely spaced in energy, such that the corresponding RE_v values are 3.19, 2.71, 2.48, and 2.36 eV, for the A, B, C, and D

states, respectively. Vibrational relaxation of the A–C states following vertical electron transfer has only a small effect on the excitation energies, resulting in small Franck–Condon effects. The corresponding Franck–Condon energies (E_{FC}) are obtained from the energy differences between the vertically formed and fully optimized states (Table 2), e.g., 3.6, 6.8, and, 8.5 kJ mol^{-1} for the A, B, and C states, respectively. Given the low Franck–Condon energies, the vibrational energy in vertically formed **1** is mainly determined by the precursor ion internal energy and is independent of the particular radical electronic state. For **1$^+$** produced by gas-phase protonation with H_3O^+, the ion internal energy is a fraction of the reaction exothermicity resulting from the difference in the

proton affinities, $-\Delta H_{rxn} = \Delta PA = PA(CH_3OCH_3) - PA(H_2O) = 104\,kJ\,mol^{-1}$ [48]. A complete equipartition of the reaction energy between $\mathbf{1}^+$ and the water molecule would result in vibrational excitation in the ion equal to $0.68 \times 104 = 71\,kJ\,mol^{-1}$, as follows from the corresponding gas-phase heat capacities. The upper limit for vibrational transfer to $\mathbf{1}^+$ is about 80% of ΔPA ($83\,kJ\,mol^{-1}$) as predicted by reaction dynamics calculations [49]. However, because ions $\mathbf{1}^+$ are formed in a regular chemical ionization ion source, the excess internal energy can be dissipated in several tens of collisions with the reagent gas (e.g., water) that the ions undergo during the residence time in the source. Hence, the lower limit for the internal energy of $\mathbf{1}^+$ is given by its rovibrational enthalpy, which is $21\,kJ\,mol^{-1}$ at 473 K. These energy estimates are important, because the lifetime of $\mathbf{1}$-OD was shown to increase dramatically with the precursor ion internal energy, as determined by the protonation exothermicity.

The excited state energies combined with the thermal energy in the radicals allow one to interpret the results of the previously reported laser photoionization measurements that found a small fraction of $\mathbf{1}$ that were ionized at the combined 488 nm (2.54 eV) and 514.5 nm (2.41 eV) wavelengths [22]. The ionization energies in Table 2 show that the A state cannot be photoionized at 488 nm, whereas the C and higher states can. Ionization of the B state is uncertain but possible, because the difference between the calculated ionization energy and photon energy (0.12 eV) is within the accuracy limits of TD-B3LYP calculations [47].

Table 2 also shows the calculated radiative lifetimes (τ) for the excited states of $\mathbf{1}$. The A state is long lived both in the equilibrium geometry ($\tau = 29\,\mu s$) and when formed by vertical electron transfer ($\tau = 17\,\mu s$) and should be relevant to affect dissociations of $\mathbf{1}$. The B state also shows kinetically relevant radiative lifetimes, e.g., 0.4 and $0.5\,\mu s$ for the relaxed and vertically formed radicals, respectively. By contrast, the C, D, and E states show 33–70 ns lifetimes for radiative transition to the repulsive X state of $\mathbf{1}$, and so if formed, they are expected to emit a photon and dissociate by O–H bond cleavage within nanoseconds. It

follows from this analysis that the metastability and C–O bond dissociations of $\mathbf{1}$ are most likely due to the formation of the A and B excited states. Therefore, the potential energy surfaces of these states were studied in more detail.

3.3. Dissociations occurring from the A and B states

The potential energy surfaces along the O–H coordinate in $\mathbf{1}$ are shown in Fig. 3. The X state is repulsive, so that radicals $\mathbf{1}$ dissociate without barrier on this potential energy surface. In contrast, the A, B, and C states are strongly bound along the O–H coordinate and show substantial potential energy increase upon stretching the O–H bond. The potential energy surfaces of the A, B, and C states along the O–H coordinate are virtually parallel and show that electron excitation from the 9a′ orbital completely removes the antibonding interaction within the hydroxyl group. The potential energy surface of the A state in $\mathbf{1}$ converges to the $^1B_1$ excited state of dimethyl ether, which by TD-B3LYP calculations is 6.14 eV above the $(CH_3)_2O$ $^1A_1$ ground state and $377\,kJ\,mol^{-1}$ above the A state of $\mathbf{1}$. Likewise, the potential energy surfaces of the B and C states in $\mathbf{1}$ converge to the $^1A_2$ and higher singlet excited states of dimethyl ether.

Investigations of potential energy surfaces along the O–C coordinate in $\mathbf{1}$ found a very different picture (Fig. 4). Both the X and A states show small potential energy increases upon stretching one of the O–C bonds in $\mathbf{1}$. The A state displays a $2\,kJ\,mol^{-1}$ barrier at a bond length of $d(\text{O–C}) = 1.60\,\text{Å}$, followed by a dip in the potential energy surface at $d(\text{O–C}) = 1.70\,\text{Å}$ and further increase at larger $d(\text{O–C})$. The X state shows a potential energy increase up to $d(\text{O–C}) = 1.675\,\text{Å}$, followed by a decrease at larger $d(\text{O–C})$. This behavior is indicative of an avoided crossing of the X and A potential energy surfaces [23] in the critical region of O–C bond stretch around 1.7 Å. Efforts were made to pinpoint the avoided crossing by complete active space (CASSCF) calculations [50]. However, CASSCF does not work well for electronic systems in which the active space includes occupied orbitals of widely different energies, such as the 8a′
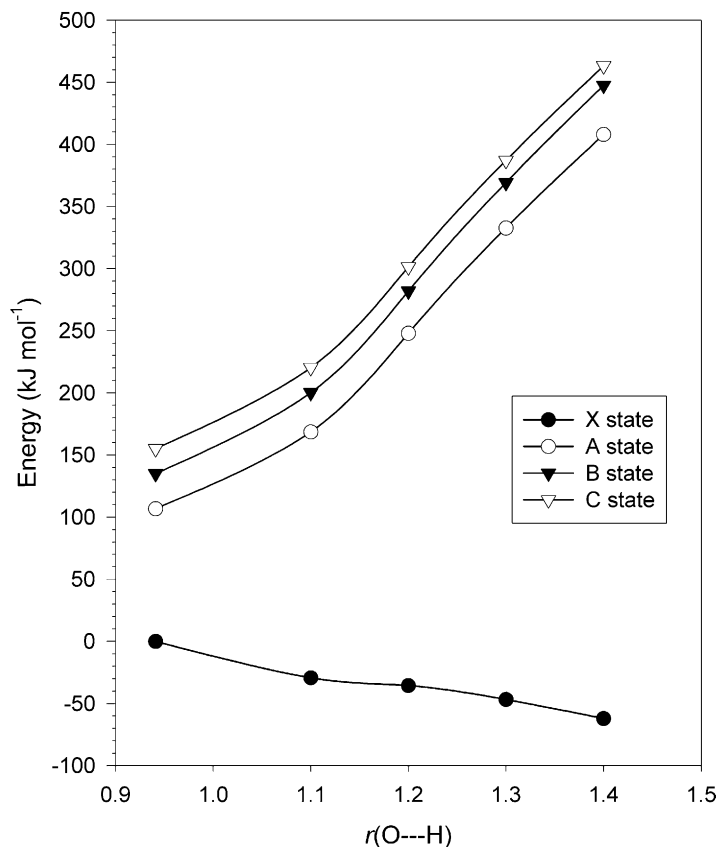
Fig. 3. UCIS/6-311++G(3df,2p) potential energy surfaces of the X, A, B, and C states along the O–H coordinate in **1**.

and 9a′ orbitals in **1**, whereas the excitation energies, e.g., 9a′ → 10a′, are much smaller.

The presence of an avoided crossing along the O–C coordinate explains the dissociation by loss of methyl. When formed by vertical electron transfer, the A state is expected to rapidly overcome the small potential energy barrier along the O–C coordinate and cross to the repulsive part of the X state potential energy surface. The overall energetics for the loss of methyl is determined by the enthalpy difference between the $CH_3OH + CH_3$ products and the A state as $\Delta H_r = (-201 + 146) - 245 = -300 \text{ kJ mol}^{-1}$. The unimolecular rate constant for the surface crossing is very likely comparable to or greater than the rate constant for radiative transition $k_{rad} \approx 1/t = 5.9 \times 10^4 \text{ s}^{-1}$. Hence, the parallel dissociations of **1** by loss of the oxonium

H and CH_3 do not proceed as competing dissociations, but originate from different electronic states of **1**, as populated by vertical electron transfer. Because the loss of H and CH_3 should be specific for the X and A states, respectively, as indicated by the calculated potential energy surfaces, the apparent branching ratio reflects the populations of the X and A states.

The B and C states are bound along the O–C coordinate and do not show signs of avoided crossing to the lower electronic states. The B state has a microsecond radiation lifetime which, together with its stability in both dissociation coordinates, makes it a good candidate for the fraction of metastable **1** that are found in the NR mass spectrum to survive for a few microseconds. This fraction is particularly affected by isotope effects (Fig. 1) that are discussed next.
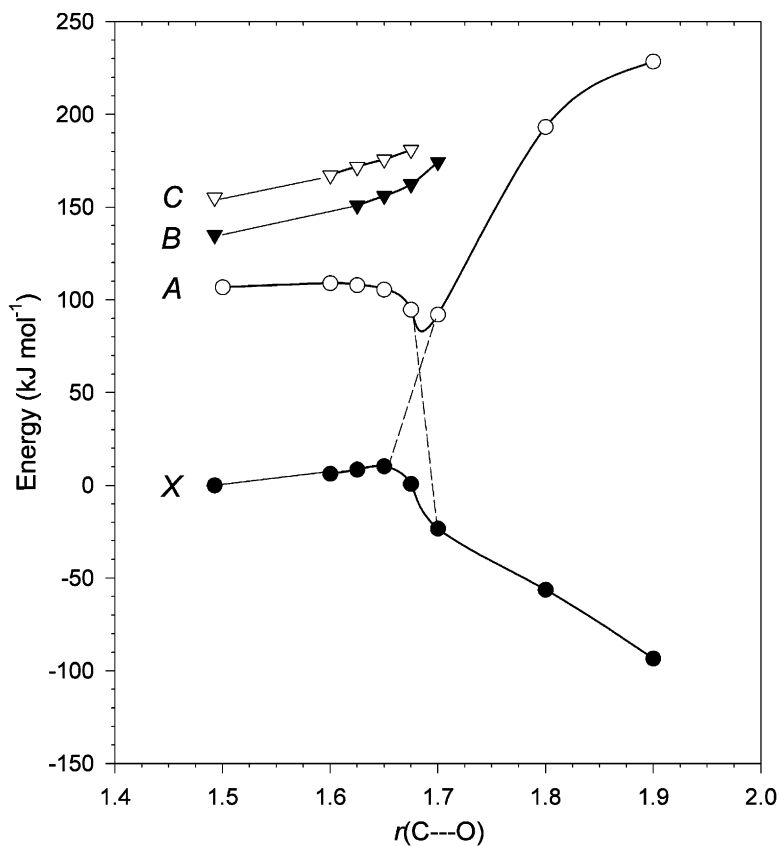
Fig. 4. UCIS/6-311++G(3df,2p) potential energy surfaces of the X, A, B, and C states along the O–C coordinate in **1**.

3.4. Temperature and isotope effects

The fraction of metastable dimethyloxonium radicals that give rise to survivor ions in the NR mass spectra is very much affected by the presence of deuterium in the precursor ion and by the ion internal energy. In the absence of deuterium, radical **1** undergoes complete dissociation. Even in the presence of deuterium, such as in **1**-OD, the fraction of metastable radicals increases dramatically when the precursor ion was prepared with substantial vibrational excitation, such as by the $104\,\text{kJ}\,\text{mol}^{-1}$ exothermic protonation with D_3O^+ in the gas phase [19].

Inspection of the NR mass spectra in Fig. 1 reveals the following facts. Both the CH_3OH and $(CH_3)_2O$ molecules formed by dissociation of **1** have substantial internal energies. This is deduced from the [m/z 31]/[m/z 32] and [m/z 45]/[m/z 46] ion intensity ratios that are lower than those in the corresponding NR mass spectra of methanol and dimethyl ether, respectively [51]. Because loss of H from the methyl group is the lowest energy dissociation that requires 91–$92\,\text{kJ}\,\text{mol}^{-1}$ in both $CH_3OH^{\bullet+}$ and $(CH_3)_2O^{\bullet+}$ [51], the large [m/z 31]/[m/z 32] and [m/z 45]/[m/z 46] ion intensity ratios indicate that large fractions of the ions must have internal energies exceeding the dissociation threshold. Of this energy, about $20\,\text{kJ}\,\text{mol}^{-1}$ results from Franck–Condon effects on vertical ionization [51], leaving $>70\,\text{kJ}\,\text{mol}^{-1}$ in the neutral molecules produced by dissociation of **1**. This is substantially less energy than produced by the exothermic dissociations of **1** (vide supra), indicating that most of the dissociation exothermicity went into the product translational energy. This conclusion is consistent

with the dissociations starting from the repulsive part of the potential energy surface, implying inefficient energy conversion to the internal vibrational modes of the products. Unfortunately, the NR mass spectra do not provide information on the rotational states of the products, and so the extent of rotational excitation cannot be estimated.

Compared to **1**, the dissociation products of **1**-OD show a slightly increased proportion of $(CH_3)_2O$ as evidenced by the peaks at m/z 46 and 45. The $[m/z\ 32]/[m/z\ 33]$ ratio corresponding to reionized $CH_3OD^{\bullet+}$ is similar to that in reionized $CH_3OH^{\bullet+}$ from **1**. The NR mass spectrum of **1**-OD indicates that the substantial fraction of metastable **1**-OD does not result from blocking one of the dissociation channels. This conclusion is consistent with the repulsive nature of the X state dissociating by loss of H or D, and the extremely low activation energy for the methyl loss from the A state for which only small isotope effects can be expected. Rather, it appears that metastable **1**-OD originates from a radiatively long-lived and bound electronic state of **1** which is either populated more efficiently from vibrationally hot **1**-OD$^+$, or whose lifetime is extended by isotope effects and vibrational excitation.

The effects on radiative lifetimes of vibrational excitation in **1**-OD were investigated as follows. First, vibrational modes involving substantial displacements of the oxonium hydrogen in **1**$^+$ were identified as the out-of-plane OH bends (3a′ and 4a′), and in-plane bend (3a″) with uncorrected wavenumbers of 712, 815, and 1101 cm^{-1}, respectively (Table 3). These are shifted to 568, 785, and 874 cm^{-1}, respectively, in **1**-OD$^+$. Assuming 104 kJ mol^{-1} vibrational excitation in **1**$^+$ and **1**-OD$^+$, the isotopically lowered vibrational frequencies in **1**-OD$^+$ result in a higher population of excited vibrational states with $v' \geq 0$. Calculations using Dunbar's equilibrium formula [52] showed that, for example, at an effective temperature of 1240 K, corresponding to 104 kJ mol^{-1} vibrational enthalpy in **1**$^+$, 45% of the 3a′ modes were in $v' \geq 1$ states, whereas the same analysis for the 3a′ mode in **1**-OD$^+$ gave 65%. Next, the potential energy for the 3a′, 4a′ and 3a″ modes were approximated by har-

monic potentials and the most probable displacements along each normal coordinate were calculated for the $v' = 1$–4 states. The corresponding non-equilibrium geometries were vertically neutralized, and radiative lifetimes were calculated for the A–E excited states. These calculations, albeit crude, showed no large effects of vibrational excitation on the radiative lifetimes of the bound and potentially metastable B–E states of **1**, as the τ values remained within $\pm 20\%$ of those for B–E states formed from vibrationally relaxed **1**$^+$. The same conclusion was reached for vibrational excitation in **1**-OD$^+$, that also indicated no substantial effects on the radiative lifetimes in the B–E electronic states of vertically neutralized **1**-OD.

Because the radiative lifetimes failed to explain the isotope effects, we examined non-radiative coupling of adjacent potential energy surfaces and its effect on the transition from the bound B state to the dissociative A state. The rate for non-radiative decay Γ is given by Fermi's golden rule [53] (Eq. (1)):

$$\Gamma = \frac{2\pi}{\hbar} \left| \langle A \left| \frac{\partial H}{\partial Q} \right| B \rangle \right|^2 \rho_A \tag{1}$$

where ρ_A is the density of the final vibrational states of the A state surface and $\langle B|$ and $|A\rangle$ are the corresponding wave functions. In order for Γ to be symmetry-invariant and because of the A (a′) and B (a″) state symmetries, the coupling coordinate Q must be of an a″ symmetry, which points to the 2a″, 3a″, 5a″–8a″ vibrational modes in **1** and the 2a″, 3a″, and 5a″ modes in **1**-OD. Assuming that the A state densities are similar for **1** and **1**-OD, a difference in the non-radiative decay of the B state in **1** and **1**-OD would have to be due to different coupling terms in Eq. (1). This is indeed indicated by the different nature of the 6a″, 7a″ and 8a″ modes in **1**-OD that do not involve displacements of the deuterium atom, so that the corresponding coordinates are inactive. Hence, we expect a less efficient vibronic coupling of the A and B states in **1**-OD than in **1** resulting in a longer lifetime for the bound B state and corresponding increase in the lifetime of **1**-OD.

It should be noted that the decreased vibronic coupling between the A and B states in **1**-OD is only one of

Table 3
Harmonic frequencies in 1^+, 1-OD$^+$, 1, and 1-OD

Species	Method[a]	Harmonic frequencies (cm^{-1})
1^+	MP2	157 (1a″), 226 (1a′), 347 (2a′), 712 (3a′), 815 (4a′), 923 (2a″), 1101 (3a″), 1159 (4a″), 1219 (5a′), 1283 (6a′), 1439 (5a″), 1482 (6a″), 1508 (7a′), 1508 (7a″), 1514 (8a″), 1523 (8a′), 1528 (9a′), 3149 (10a′), 3150 (9a″), 3284 (11a′), 3285 (10a″), 3297 (11a″), 3298 (12a′), 3711 (13a′)
1^+-OD	MP2	157 (a″), 222 (a′), 346 (a′), 568 (a′), 785 (a′), 874 (a″), 977 (a″), 1159 (a″), 1218 (a′), 1247 (a″), 1272 (a′), 1480 (a″), 1506 (a′), 1508 (a′), 1511 (a″), 1523 (9a′), 1527 (a′), 2705 (a′), 3149 (a′), 3150 (a″), 3284 (a′), 3285 (a″), 3297 (a″), 3298 (a′)
1^+-D$_6$	MP2	112 (a″), 175 (a′), 301 (a′), 685 (a′), 742 (a′), 828 (a″), 862 (a″), 942 (a″), 967 (a′), 1062 (a′), 1088 (a″), 1094 (a″), 1100 (a′), 1102 (a′), 1103 (a″), 1142 (a′), 1410 (a″), 2250 (a′), 2250 (a″), 2445 (a″), 2445 (a′), 2454 (a″), 2456 (a′), 3711 (a′)
1^+-OD, D$_6$	MP2	112 (a″), 171 (a′), 300 (a′), 544 (a′), 723 (a′), 804 (a″), 843 (a″), 904 (a″), 961 (a′), 1035 (a′), 1085 (a″), 1093 (a″), 1098 (a″), 1100 (a′), 1102 (a′), 1127 (a″), 1141 (a′), 2250 (a′), 2250 (a″), 2445 (a″), 2445 (a′), 2453 (a″), 2456 (a′), 2705 (a′)
2	B3LYP	21 (a′), 39 (a″), 100 (a′), 202 (a″), 236 (a′), 410 (a′), 937 (a′), 1118 (a″), 1161 (a″), 1192 (a′), 1195 (a″), 1266 (a′), 1460 (a″), 1481 (a″), 1486 (a′), 1490 (a′), 1494 (a″), 1512 (a′), 2961 (a″), 2972 (a′), 3005 (a′), 3010 (a″), 3109 (a″), 3110 (a′)
3	B3LYP	i920 (a″), 64 (a″), 92 (a″), 178 (a′), 258 (a′), 417 (a′), 702 (a″), 718 (a′), 742 (a″), 812 (a′), 1067 (a″), 1083 (a′), 1147 (a″), 1437 (a″), 1439 (a′), 1443 (a″), 1444 (a′), 3090 (a′), 3090 (a″), 3226 (a′), 3226 (a″), 3241 (a′), 3241 (a″), 3771 (a′)
(A) 1	UCIS	126 (a″), 203 (a′), 336 (a′), 634 (a″), 642 (a′), 750 (a′), 1160 (a″), 1226 (a″), 1286 (a′), 1334 (a′), 1532 (a″), 1562 (a″), 1584 (a″), 1585 (a′), 1589 (a″), 1590 (a′), 1601 (a′), 3199 (a″), 3201 (a′), 3342 (a′), 3342 (a″), 3367 (a″), 3369 (a′), 4349 (a′)
(A) 1-OD	UCIS	126 (a″), 200 (a′), 332 (a′), 524 (a′), 616 (a″), 709 (a′), 1011 (a″), 1226 (a″), 1285 (a′), 1323 (a″), 1326 (a′), 1558 (a″), 1576 (a″), 1585 (a′), 1588 (a″), 1590 (a′), 1599 (a′), 3167 (a′), 3199 (a″), 3202 (a′), 3342 (a″), 3342 (a′), 3366 (a″), 3370 (a′)
(A) 1-D$_6$	UCIS	90 (a″), 159 (a′), 293 (a′), 617 (a′), 623 (a″), 695 (a′), 893 (a″), 923 (a″), 1010 (a′), 1083 (a′), 1138 (a″), 1148 (a′), 1151 (a″), 1156 (a′), 1159 (a″), 1192 (a′), 1507 (a″), 2285 (a″), 2286 (a′), 2489 (a″), 2492 (a′), 2510 (a″), 2512 (a′), 4348 (a′)
(A) 1-OD, D$_6$	UCIS	90 (a″), 155 (a′), 291 (a′), 504 (a′), 607 (a″), 656 (a′), 847 (a″), 922 (a″), 1007 (a′), 1065 (a′), 1135 (a″), 1141 (a″), 1148 (a′), 1155 (a′), 1156 (a″), 1193 (a′), 1195 (a″), 2285 (a″), 2286 (a′), 2489 (a″), 2492 (a′), 2509 (a″), 2512 (a′), 3167 (a′)
(B) 1	UCIS	156 (a″), 231 (a′), 349 (a′), 665 (a′), 831 (a″), 963 (a″), 1175 (a″), 1244 (a″), 1298 (a′), 1373 (a′), 1541 (a″), 1566 (a″), 1592 (a″), 1593 (a′), 1602 (a′), 1606 (a″), 1613 (a′), 3215 (a″), 3215 (a′), 3344 (a″), 3348 (a′), 3359 (a″), 3367 (a′), 4395 (a′)
(B) 1-OD	UCIS	156 (a″), 226 (a′), 345 (a′), 525 (a′), 816 (a′), 927 (a″), 1032 (a″), 1244 (a″), 1297 (a′), 1351 (a″), 1364 (a′), 1553 (a″), 1582 (a″), 1593 (a′), 1595 (a″), 1602 (a′), 1613 (a′), 3202 (a′), 3215 (a″), 3216 (a′), 3344 (a″), 3349 (a″), 3358 (a″), 3368 (a′)
(B) 1-D$_6$	UCIS	111 (a″), 180 (a′), 305 (a′), 644 (a′), 766 (a′), 875 (a″), 922 (a″), 997 (a″), 1016 (a′), 1119 (a′), 1123 (a″), 1153 (a′), 1155 (a′), 1155 (a″), 1179 (a″), 1215 (a′), 1533 (a″), 2294 (a″), 2298 (a′), 2490 (a″), 2494 (a′), 2503 (a″), 2511 (a′), 4395 (a′)
(B) 1-OD, D$_6$	UCIS	111 (a″), 173 (a′), 298 (a′), 498 (a′), 748 (a′), 856 (a″), 890 (a″), 951 (a″), 1004 (a′), 1089 (a′), 1123 (a″), 1152 (a′), 1152 (a″), 1155 (a′), 1161 (a″), 1205 (a″), 1215 (a′), 2294 (a″), 2298 (a′), 2489 (a″), 2494 (a′), 2502 (a″), 2511 (a′), 3182 (a′)
(C) 1	UCIS	133 (a″), 224 (a′), 378 (a′), 758 (a′), 851 (a′), 969 (a″), 1188 (a″), 1257 (a″), 1320 (a′), 1384 (a′), 1559 (a″), 1584 (a″), 1591 (a′), 1560 (a″), 1610 (a′), 1628 (a′), 1638 (a″), 3229 (a′), 3229 (a″), 3349 (a′), 3353 (a″), 3380 (a″), 3383 (a′), 4394 (a′)
(C) 1-OD	UCIS	133 (a″), 223 (a′), 374 (a′), 597 (a′), 826 (a′), 923 (a″), 1054 (a″), 1257 (a″), 1317 (a′), 1372 (a′), 1390 (a″), 1563 (a″), 1588 (a″), 1589 (a′), 1607 (a″), 1610 (a′), 1628 (a′), 3201 (a′), 3229 (a′), 3229 (a″), 3349 (a′), 3353 (a″), 3380 (a″), 3383 (a′)
(C) 1-D$_6$	UCIS	95 (a″), 179 (a′), 326 (a′), 722 (a′), 779 (a′), 880 (a″), 932 (a′), 1009 (a″), 1044 (a′), 1133 (a′), 1137 (a″), 1149 (a′), 1162 (a″), 1168 (a′), 1172 (a″), 1226 (a′), 1582 (a″), 2305 (a″), 2308 (a′), 2495 (a′), 2497 (a″), 2518 (a′), 2518 (a′), 4394 (a′)
(C) 1-OD, D$_6$	UCIS	95 (a″), 175 (a′), 319 (a′), 566 (a′), 754 (a′), 865 (a″), 889 (a″), 959 (a″), 1025 (a′), 1095 (a′), 1136 (a″), 1148 (a′), 1160 (a″), 1161 (a″), 1165 (a′), 1226 (a′), 1252 (a″), 2305 (a″), 2308 (a′), 2495 (a′), 2497 (a″), 2516 (a″), 2518 (a′), 3180 (a′)

[a] MP2 and UCIS frequency calculations with the 6-31++G(2d,p) basis set, B3LYP frequency calculations with the 6-311++G(2df,p) basis set.

the possible explanations of the radical metastability. Because of the bound nature of higher excited electronic states in **1**, isotope effects on the population of such states upon vertical electron transfer could also enhance the fraction of metastable **1**-OD. However, the physical nature of such isotope effects remains unclear.

4. Conclusions

The analysis of the electronic states in the hypervalent radical **1** allows us to arrive at the following conclusions. The X state is repulsive and dissociates without barrier by cleavage of the O–H bond, which is observed as loss of hydrogen in the NR mass spectrum. The loss of methyl, which is also observed in the NR mass spectrum, proceeds from the A state of **1** by crossing to the repulsive part of the X state. The fraction of metastable radicals, as observed for **1**-OD, originates from long-lived B and higher electronic states of **1**. These states are bound in the O–H and O–C coordinates. The large isotope effects on metastability in **1**-OD are explained by lower rates of non-radiative transfer from the bound B state to the dissociative A state. The gas-phase chemistry of dimethyloxonium radical **1** resembles that of the dimethylammonium radical, $(CH_3)_2NH_2^\bullet$, which also shows state-selective metastability and reactivity in the ground and excited electronic states.

References

[1] G.N. Lewis, J. Am. Chem. Soc. 38 (1916) 762.
[2] C.W. Perkins, J.C. Martin, A.J. Arduengo, W. Lau, A. Alegria, J.K. Kochi, J. Am. Chem. Soc. 102 (1980) 7753.
[3] A.E. Reed, P.V.R. Schleyer, J. Am. Chem. Soc. 112 (1990) 1434.
[4] K. Akiba, Chemistry of Hypervalent Compounds, Wiley-VCH, New York, 1999.
[5] C.H. Schiesser, L.M. Wild, Tetrahedron 37 (1996) 13265.
[6] K.F. Ferris, J.A. Franz, C. Sosa, R.J. Bartlett, J. Org. Chem. 57 (1992) 777.
[7] B.W. Wiliams, R.F. Porter, J. Chem. Phys. 73 (1980) 5598.
[8] G.I. Gellene, D.A. Cleary, R.F. Porter, J. Chem. Phys. 77 (1982) 3471.
[9] G.I. Gellene, R.F. Porter, J. Chem. Phys. 81 (1984) 5570.
[10] S.-J. Jeon, A.B. Raksit, G.I. Gellene, R.F. Porter, J. Am. Chem. Soc. 107 (1985) 4129.
[11] C.W. Perkins, R.B. Clarkson, J.C. Martin, J. Am. Chem. Soc. 108 (1986) 3206.
[12] C. Wesdemiotis, R. Feng, F.W. McLafferty, J. Am. Chem. Soc. 108 (1986) 5656.
[13] A.B. Raksit, R.F. Porter, J. Chem. Soc., Chem. Commun. (1987) 500.
[14] S.F. Selgren, G.I. Gellene, J. Phys. Chem. 87 (1987) 5804.
[15] J.L. Holmes, M. Sirois, Org. Mass Spectrom. 25 (1990) 481.
[16] C. Wesdemiotis, A. Fura, F.W. McLafferty, J. Am. Soc. Mass Spectrom. 2 (1991) 459.
[17] M. Gu, F. Turecek, J. Am. Chem. Soc. 114 (1992) 7146.
[18] S.A. Shaffer, F. Turecek, J. Am. Chem. Soc. 116 (1994) 8647.
[19] M. Sirois, M. George, J.L. Holmes, Org. Mass Spectrom. 29 (1994) 11.
[20] S.A. Shaffer, F. Turecek, J. Am. Soc. Mass Spectrom. 6 (1995) 1004.
[21] S.A. Shaffer, M. Sadílek, F. Turecek, J. Org. Chem. 61 (1996) 5234.
[22] M. Sadilek, F. Turecek, J. Phys. Chem. 100 (1996) 9610.
[23] M. Sadilek, F. Turecek, J. Phys. Chem. 100 (1996) 15027.
[24] V.Q. Nguyen, M. Sadilek, A.J. Frank, J.G. Ferrier, F. Turecek, J. Phys. Chem. A 101 (1997) 3789.
[25] J.K. Wolken, V.Q. Nguyen, F. Turecek, J. Mass Spectrom. 32 (1997) 1162.
[26] L. Frøsig, F. Turecek, J. Am. Soc. Mass Spectrom. 9 (1998) 242.
[27] H. Cardy, D. Liotard, A. Dargelos, E. Poquet, Chem. Phys. 77 (1983) 287.
[28] J. Kaspar, V.H. Smith Jr., B.N. McMaster, Chem. Phys. 96 (1985) 81.
[29] E. Kassab, E.M. Evleth, J. Am. Chem. Soc. 109 (1987) 1653.
[30] A. Demolliens, O. Eisenstein, P.C. Hiberty, J.M. Lefour, G. Ohanessian, S.S. Shaik, F. Volatron, J. Am. Chem. Soc. 111 (1989) 5623.
[31] A.I. Boldyrev, J. Simons, J. Chem. Phys. 97 (1992) 6621.
[32] A.I. Boldyrev, J. Simons, J. Chem. Phys. 99 (1993) 4628.
[33] J.S. Wright, D. McKay, J. Phys. Chem. 100 (1996) 7392.
[34] A.I. Boldyrev, J. Simons, J. Phys. Chem. 96 (1992) 8840.
[35] P.W. McLoughlin, G.I. Gellene, J. Phys. Chem. 96 (1992) 4396.
[36] J.K. Park, Chem. Phys. Lett. 315 (1999) 119.
[37] D. Talbi, R.P. Saxon, J. Chem. Phys. 91 (1989) 2376.
[38] (a) F.W. Chen, E.R. Davidson, J. Phys. Chem. A 105 (2001) 10915. For other recent calculations of the H_3O system see;
      (b) H. Tachikawa, T. Yamano, Chem. Phys. Lett. 335 (2001) 305;

(c) M.H. Cohen, J. Seitzinger, M.D. Tissandier, J.V. Coe, J. Chem. Phys. 110 (1999) 11113;

(d) M. Luo, M. Jungen, Chem. Phys. 241 (1999) 297;

(e) A.E. Ketvirtis, J. Simons, J. Phys. Chem. A 103 (1999) 6552;

(f) C. Lavin, I. Martin, Adv. Quantum Chem. 28 (1997) 205.

[39] G. Herzberg, Faraday Discuss. R. Soc. Chem. 71 (1981) 165.

[40] M. Larsson, Int. J. Mass Spectrom. Ion Processes 149/150 (1995) 403.

[41] B.R. Rowe, J.B. Mitchell, A. Canosa (Eds.), Dissociative Recombination. Theory, Experiment, and Applications, Plenum Press, New York, 1993.

[42] G.I. Gellene, R.F. Porter, Acc. Chem. Res. 16 (1983) 200.

[43] For reviews see: (a) C. Wesdemiotis, F.W. McLafferty, Chem. Rev. 87 (1987) 485;

(b) J.K. Terlouw, H. Schwarz, Angew. Chem. Int. Ed. Engl. 26 (1987) 805;

(c) J.L. Holmes, Mass Spectrom. Rev. 3 (1989) 513;

(d) J.K. Terlouw, Adv. Mass Spectrom. 11 (1989) 984;

(e) F.W. McLafferty, Science 247 (1990) 925;

(f) F. Turecek, Org. Mass Spectrom. 27 (1992) 1087;

(g) N. Goldberg, H. Schwarz, Acc. Chem. Res. 27 (1994) 347;

(h) C.A. Schalley, G. Hornung, D. Schroder, H. Schwarz, Chem. Soc. Rev. 27 (1998) 91;

(i) F. Turecek, J. Mass Spectrom. 33 (1998) 779;

(j) D.V. Zagorevskii, J.L. Holmes, Mass Spectrom. Rev. 18 (1999) 87.

[44] M.J. Frisch, G.W. Trucks, H.B. Schlegel, G.E. Scuseria, M.A. Robb, J.R. Cheeseman, V.G. Zakrzewski, J.A. Montgomery, R.E. Stratmann, J.C. Burant, S. Dapprich, J.M. Millam, A.D. Daniels, K.N. Kudin, M.C. Strain, O. Farkas, J. Tomasi, V. Barone, M. Cossi, R. Cammi, B. Mennucci, C. Pomelli, C. Adamo, S. Clifford, J. Ochterski, G.A. Petersson, P.Y. Ayala, Q. Cui, K. Morokuma, D.K. Malick, A.D. Rabuck, K. Raghavachari, J.B. Foresman, J. Cioslowski, J.V. Ortiz, B.B. Stefanov, G. Liu, A. Liashenko, P. Piskorz, I. Komaromi, R. Gomperts, R.L. Martin, D.J. Fox, T. Keith, M.A. Al-Laham, C.Y. Peng, A. Nanayakkara, C. Gonzalez, M. Challacombe, P.M.W. Gill, B.G. Johnson, W. Chen, M.W. Wong, J.L. Andres, M. Head-Gordon, E.S. Replogle and J.A. Pople, Gaussian 98, Revision A.6, Gaussian, Inc., Pittsburgh, PA, 1998.

[45] (a) A.D. Becke, J. Chem. Phys. 98 (1993) 1372;

(b) A.D. Becke, J. Chem. Phys. 98 (1993) 5648;

(c) P.J. Stephens, F.J. Devlin, C.F. Chabalowski, M.J. Frisch, J. Phys. Chem. 98 (1994) 11623.

[46] J.B. Foresman, M. Head-Gordon, J.A. Pople, M.J. Frisch, J. Phys. Chem. 96 (1992) 135.

[47] R.E. Stratmann, G.E. Scuseria, M.J. Frisch, J. Chem. Phys. 109 (1998) 8218.

[48] NIST Standard Reference Database No. 69., February 2000 Release. http//:webbook.nist.gov.

[49] E. Uggerud, Adv. Mass Spectrom. 13 (1995) 53.

[50] R.H.E. Eade, M.A. Robb, Chem. Phys. Lett. 83 (1981) 362.

[51] V.Q. Nguyen, F. Turecek, J. Mass Spectrom. 31 (1996) 843.

[52] R.C. Dunbar, J. Chem. Phys. 90 (1989) 7369.

[53] G. Fischer, Vibronic Coupling, Academic Press, London, 1984, pp. 29–52.